Int. J. Electrochem. Sci., 13 **(2018)** 9359 – 9373, doi: 10.20964/2018.10.11

International Journal of
ELECTROCHEMICAL
SCIENCE
www.electrochemsci.org

Synthesis of a Conductive Pt-Bi/CAG composite and its application for Methyl Orange Decolorization

Lin Li[1], *Jin-lei Xiong*[1], *Luo-chun Wang*[1,*], *Tian Xin-mei*[1], *Zi-yang Lou*[2], *Shou-qiang Huang*[2] , *Zhen Zhou*[1]

[1] College of Environmental and Chemical Engineering, Shanghai University of Electric Power, Shanghai 200090, China,
[2] School of Environmental Science and Engineering, Shanghai Jiao Tong University, Shanghai 200240, China
[*]E-mail: wangluochun@shiep.edu.cn

Received: 4 June 2018 / *Accepted:* 16 July 2018 / *Published:* 1 September 2018

To improve the electrochemical properties of electrodes and reduce their cost, a special multi-layer matrix was synthesized as an electrode material, which was composed of cement, active carbon (AC), and graphite with Pt-Bi co-deposition (Pt-Bi/CAG). Pt-Bi particles were found to be homogeneously distributed on the surface of the GAC electrode according to the SEM, EDS and XRD patterns, and the Pt-Bi/CAG-G5 electrode, which was made up of 5% graphite, 20% AC powder, 25% cement and 50% water, showed the best electrochemical performance in terms of specific capacitance, corrosion resistance and catalytic performance. The specific capacitance of the Pt-Bi/CAG-G5 electrode was 1.103 times larger than that of the Pt-Bi/CAG-G7.5 electrode, and the corrosion resistance was slightly lower than that of the Pt-Bi/CAG-G0 electrode. The current density was appreciably larger than those of all other electrodes, and it was 1.5 times larger than that of the Pt-Bi/CAG-G7.5 electrode. Next, the electrode was optimized based on methyl orange (MO) decoloration experiments, and approximately 76.62% of the decoloration rate was obtained by the Pt-Bi/CAG-G5 electrode, with a corresponding TOC removal rate of 54.80% in 180 min under a square wave potential (E_U 1.5 V, E_L −1.5 V). This composite electrode provides a cost-efficient application using electrochemical technologies (ETs) for the removal of refractory compounds.

Keywords: cement/AC/graphite electrode; electrochemical properties; multi-layer-matrix; cost-efficiency

1. INTRODUCTION

Electrodes are essential components of electrochemical technologies (ETs), and the development of electroactive materials used in the manufacture of electrodes plays a significant role in

improving electrochemical performance in terms of energy and power densities [1]. The high energy efficiency, amenability to automation, simple equipment required, and mild conditions of operation of ETs are basic requirements for the treatment of wastewater, especially those containing synthetic organic dyes [2]. A significant body of work has been conducted to create neoteric electrode materials, which can be categorized into carbon-based materials, such as carbon nanofibers [3], carbon xerogels [4], carbon spheres [5], carbon nanosheets [6], metal oxide-based materials including MnO_2 [7], Ni-Co [8], NiO [9], and mixed materials of carbon-metal oxide composites [10,11].

The mineralization efficiency of dyes by ETs is highly dependent on the anode, which has been confirmed by Comninellis [12]. Various electrode materials have been applied to degrade dyes, including BBD and PbO_2 [13], metal oxides doped with Ti including Ti/RuO_2, Ti/IrO_2, Ti/CuO_2, Ti/NiO_2, Ti/CoO_2 and Ti/AgO_2 [14-17], Ti/Pt [18], and carbonaceous electrodes [19]. Platinum has been considered as an efficient unique catalyst due to an exceptionally high electrochemical surface area, which enhances electrochemical catalytic activity [20]. The short-term durability periods and the release of poisonous intermediates hamper the use of platinum in practice [21]. A workable solution for minimizing its poisoning effects is to dope foreign metal atoms and modify the surface morphology [22]. Bi has been used as a favorable modifier for Pt [23]. Pt-Bi intermetallics [24], Pt-Bi and Pt_2Bi alloys [25, 26], and electro-deposited Pt-Bi [27] have been reported due to their favorable catalytic performance in electrochemical oxidation. The main limitations of ETs are their lack of energy-efficient and cost-effective scalability [28], modified Pt-Bi based anodes have been taken into consideration because the high cost of Pt-Bi intermetallics and alloys hampers their wide application.

Due to its excellent specific surface area, high porosity, and low cost (compared with metal material), active carbon (AC) has been considered as a possible electrode supporting material. However, its large-scale application is still limited due to economic considerations [29]. Combining AC with a common and cheap material is a feasible solution. Cement, as a predominant building material, can be a good option due to its high strength, mold ability, and environmentally friendly properties [30]. The good durability of cement is conducive to withstanding the corrosion of organic matter in wastewater [31]. AC can be considered as a potential additive in cementitious material to make it porous, the resultant porous cementitious material can also help to adsorb organic chemical pollutants [32]. To increase the electrical conductivity of porous AC-cement material, one of the options is to add conductive material into a cement slurry, which can accelerate electronic transmission [33]. Graphite is a favorable choice for application in the industrial product due to its good chemical inertness and oxidation resistance [34]. To improve experimental reproducibility and electrical conductivity, graphite paper can be introduced as a supporting material in the electrode.

In this study, a special porosity conductive cementitious material was synthesized based on carbon as an electrode material. This material was composed of a multi-layer-matrix of cement/AC/graphite powder by Pt-Bi co-deposition (Pt-Bi/CAG). The relationships between electrode components and electrochemical activities were explored in terms of SEM, EDS and XRD patterns. The methyl orange (MO) decoloration process was operated to test the catalytic performance, and the best ratio of the electrode material was determined by electrochemical tests. Finally, we calculated the cost of the electrode produced.

2. EXPERIMENTAL

2.1. Preparation and characterization of the Pt-Bi/CAG electrodes

The optimization of the CAG (cement, AC powder and graphite) mixture material is shown in Table 1. Before preparing the electrode, the AC powder was washed to remove the ash. Moderate deionized water was used to pretreat the AC powder, graphite and cement. A suitable amount of the slurry was added to the graphite paper and pressed into a regular and smooth surface flake by using a mold. The precursors were then placed in a cement incubator at 25℃ and 90% humidity for 3 days. The composite electrode CAG, with an active area of 20 mm × 40 mm and a thickness of 1 mm, was used as the substrate for deposition.

Table 1. Optimization proportions for Pt-Bi/CAG

	Composition content	G [a]/CAG [e] (wt.%)	A [b]/CAG (wt.%)	C [c]/CAG (wt.%)	W [d]/CAG (wt.%)
Electrode Pt-Bi/CAG-G [f]	G0	0	25	25	50
	G2.5	2.5	22.5	25	50
	G5	5	20	25	50
	G7.5	7.5	17.5	25	50
	G10	10	15	25	50
	G15	15	10	25	50
	G20	20	5	25	50
	G25	25	0	25	50
Electrode Pt-Bi/CAG-C [g]	C25	5	20	25	50
	C30	4	16	30	50
	C35	3	12	35	50
	C40	2	8	40	50
	C45	1	4	45	50
Electrode Pt-Bi/CAG-W [h]	W90	5.5	22	27.5	45
	W100	5	20	25	50
	W110	4.5	18	22.5	55

[a] G—graphite.
[b] A—AC powder.
[c] C—cement.
[d] W—water.
[e] CAG—the cement-AC-graphite powder mixture material.
[f] Pt-Bi/CAG-G—Fixing W:CAG =1:1, C:CAG=1:2.
[g] Pt-Bi/CAG-G—Fixing W:CAG=1:1, A:G=4:1.
[h] Pt-Bi/CAG-G—Fixing C:A:G=5:4:1.

The Pt-Bi/CAG was prepared by electrochemical deposition with a constant potential [35]. The compound solution prepared with 0.5 g L^{-1} H_2PtCl_6, 0.5 mM L^{-1} $Bi(NO_3)_3$, 2 g L^{-1} citric acid and 1% HNO_3 was used as the electro-deposition solution, which should be deoxygenated with nitrogen before using. The electro-deposition was operated with a three-electrode system consisting of a working electrode (the prepared Pt-Bi/CAG electrode), a counter electrode (a platinum wire), and a reference

electrode (a saturated Ag/AgCl electrode). The deposition was continued for 240 s at an applied potential of −0.8 V. The electrodeposited electrode was placed in a blast oven and dried at 40 ℃ for 2 days to obtain a multi-layer-matrix Pt-Bi/CAG composite electrode.

2.2. Electrochemical tests

A three-electrode system was used for electrochemical tests, which were conducted in 0.1 M Na_2SO_4 solution. The three-electrode system consisted of a Pt-Bi/CAG electrode (the working electrode), a titanium mesh (the counter electrode), and a saturated Ag/AgCl electrode (the reference electrode) [35]. To measure the specific capacitances of the electrodes, cyclic voltammetry (CV) was conducted at a scan rate of 0.01 V s^{-1} using the potential range from −1 V to 1 V. The specific capacitances (Cs in F cm^{-2}) of the electrodes were calculated by Eq. (1):

$$C_S = \int idV/2 \times s \times \Delta V \times SR \quad (1)$$

where $\int idV$ is the integrated area of the CV curve, s is the active area of the electrode strip (cm^2), ΔV is the potential range, and SR is the scan rate (V s^{-1}).

The polarization curve was examined to study the corrosion resistance of the catalyst with a scan rate of 0.001 V s^{-1}, assuming a measured open circuit potential and a selected self-corrosion potential. The catalytic activities of the electrodes were achieved by CV curves in the 5 mM $[Fe(CN)_6]^{3-}/[Fe(CN)_6]^{4-}$ and 0.1 M Na_2SO_4 mixture solution with a scan rate of 0.1 V s^{-1}. The chronoamperometric response curves were carried out with 20 mg/L MO to evaluate the electrocatalytic response of the electrodes in the 1.5 V upper potential (E_U) to −1.5 V lower potential (E_L) range, with a period ratio of 30 s.

2.3. MO decoloration processes

MO was conducted as the model pollution for testing the catalytic performance of the electrode. Electrochemical degradation of MO was performed in a three-electrode system, which was the same as that used in the electrochemical tests. All of the MO degradation experiments were performed under the square-wave potential with 1.5 V E_U and −1.5 V E_L [35] for 180 min in the 20 mg L^{-1} MO solution. The phosphate-buffered solution was added into the MO solution to maintain a neutral pH. All batch experiments were conducted in duplicate, and the average data were presented here. The stability of the Pt-Bi/CAG electrode was evaluated by at least 4 cycles of MO decoloration experiments. Based on pseudo-first-order kinetics, the apparent reaction rate constants (k_{obs}) of the MO decoloration processes can be obtained from the following first-order kinetics model (Eq. 2):

$$k_{obs} = \frac{\ln([MO]_0/[MO])}{t} + C \quad (2)$$

where $[MO]_0$ and [MO] represent the concentrations of the initial MO and current MO, t stands for the decoloration time, and C is a constant.

2.4. Measurement methods

The surface morphology of the Pt-Bi/CAG electrode was characterized using scanning electron microscopy, and the composition was analyzed with an energy dispersive spectrometer (FESEM, JSM-7800F, JEOL, Japan). The concentrations of MO and the degradation products of MO were measured using a UV-Vis spectrophotometer (UV-2600 PC, Shimadzu Co., Japan) and a total organic carbon analyzer (TOC, multi N/C 3100, Analytik Jena AG, Germany). The intermediate formation of MO was characterized by FTIR (FT-IR Spectrometer, Spectra Two, Perkin Elmer Co., USA). The original MO solution and the degradation solution were both extracted by an equal volume of methylene dichloride (chromatography grade). The extraction solutions were dehydrated by the use of $MgSO_4$ for 24 h, and the organic phases were then concentrated and subjected to FTIR analysis.

3. RESULTS AND DISCUSSION

3.1. Electrochemical performance of the multi-layer-matrix Pt-Bi/CAG electrode

Eight electrodes (referred to as Pt-Bi/CAG-G0 to Pt-Bi/CAG-G25) were synthesized, and their electrochemical performance was characterized and compared. The specific capacitance values at various graphite contents and with deposition are shown in Fig. 1. The good fusiform curves without significant redox peaks indicated that the ions formed a stable double layer structure on the electrode surface [36], and the specific capacitances of these Pt-Bi/CAG electrodes were proportional to the areas of the close CV curves. The specific capacitance was dependent on the graphite content. When the content of graphite was in the range of 5–15%, the specific capacitances of Pt-Bi/CAG-G5, Pt-Bi/CAG-G7.5, Pt-Bi/CAG-G10 and Pt-Bi/CAG-G20 were 36.97 F cm^{-2}, 33.52 F cm^{-2}, 24.12 F cm^{-2} and 16.36 F cm^{-2}, respectively, which were better than those of Pt-Bi/CAG-G0 (11.24 F cm^{-2}), Pt-Bi/CAG-G2.5 (12.36 F cm^{-2}), Pt-Bi/CAG-G20 (11.18 F cm^{-2}) and Pt-Bi/CAG-G25 (9.33 F cm^{-2}). This can be explained by the fact that there is a percolation threshold for graphite-cement-AC powder matrix composite material, which marks the insulator-conductor transition [37]. With the addition of graphite (0–5%), the continuous electrical conductive path begins to form. Electrons can transmit among the adjacent graphite particles by direct contact or tunneling effect, resulting in an abrupt increase in the specific capacitance. However, after reaching the maximum value for Pt-Bi/CAG-G5 (36.97 F cm^{-2}), the specific capacitance decreased with increasing graphite content. The low specific capacitance should be ascribed to the excessive graphite content (7.5–25%) which would cover the porous AC surface, hindering the transport of electrons. Fig. 1A clearly shows that the specific capacitance of the Pt-Bi/CAG-G5 electrode was the best, which was appreciably larger than those of the other electrodes and 1.103 times larger than that of the Pt-Bi/CAG-G7.5 electrode.

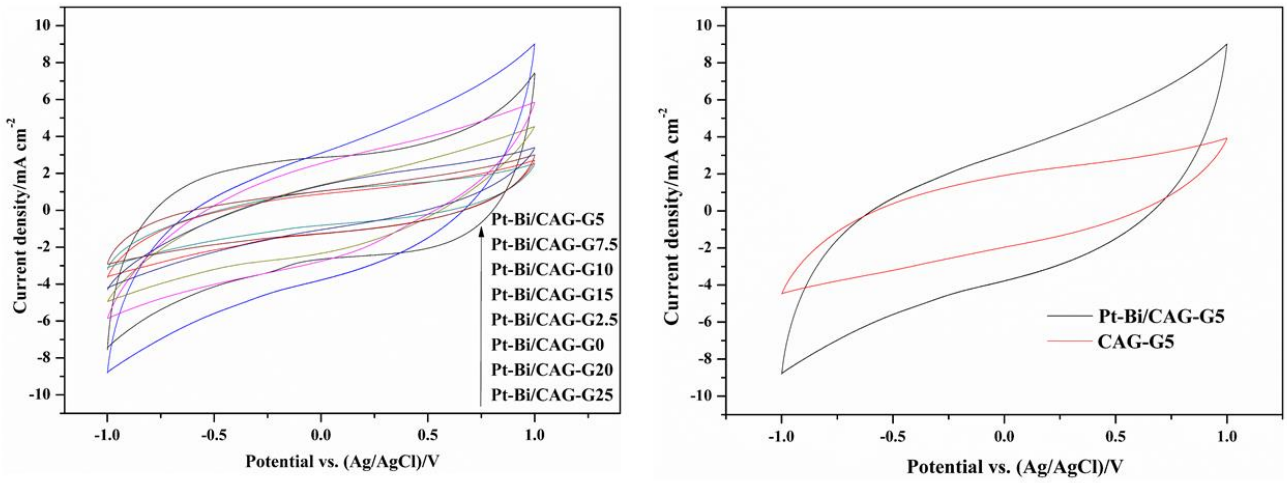

Figure 1. CV curves of the Pt-Bi/CAG electrodes in 0.1 M Na_2SO_4 solution at a scan rate of 0.01 V s^{-1} from -1.0 V to 1.0 V. A: Pt-Bi/CAG electrodes; B: Pt-Bi/CAG-G10 and CAG-G10 electrodes.

From Fig. 1B, the specific capacitances of Pt-Bi/CAG-G5 and CAG-G5 are 36.97 F cm^{-2} and 18.76 F cm^{-2}, respectively. The enhanced specific capacitance of the Pt-Bi/CAG-G5 electrode compared with the CAG-G5 electrode should be owed to the favorable conductivity of Pt-Bi and the electronic effects [25] between Pt and Bi. Furthermore, the Pt-Bi modified CAG-G5 electrode showed a higher specific capacitance than that of the RGO modified electrode (GAC-20, 7.96 F cm^{-2}) [38] and the metal-oxide-based electrode NiO-N3 (63 F g^{-1}) [9]. The uniform deposition of Pt-Bi in the Pt-Bi/CAG-G5 surface expedited the electrons transfer [39].

According to the electrochemical corrosion theory, higher corrosion potentials and lower corrosion currents favor better corrosion resistance of electrodes [40]. Fig. 2 displays the polarization curves of electrodes Pt-Bi/CAG-G0 to Pt-Bi/CAG-G25. The corrosion potential of the Pt-Bi/CAG electrodes (from G0 to G25) increased with increasing graphite content: −0.339V, −0.230V, −0.180, −0.160V, −0.120V, −0.100V, −0.078V and −0.020V, respectively, indicating better corrosion resistance. At the same time, the corrosion currents of the Pt-Bi/CAG electrodes (from G0 to G25), which were obtained at the crossing point of the tangent lines of the two curves in each polarization figure [39], were 5.247×10^{-5}, 3.933×10^{-5}, 2.418×10^{-5}, 1.032×10^{-4}, 2.152×10^{-4}, 5.143×10^{-4}, 2.286×10^{-3} and 3.175×10^{-3}, respectively, indicating increased corrosion rate with increasing graphite content. This was in accordance with the phenomenon that the corrosion resistance of the electrodes was lower with decreasing content of AC carbon, and the specific capacitances of the electrodes did not increase linearly (Fig. 1A). Generally, in terms of both corrosion potential and corrosion current, the Pt-Bi/CAG-G5 electrode was considered to be the best, which possessed satisfactory corrosion resistance ability.

Fig. 2B shows the comparison of the corrosion resistance of the Pt-Bi/CAG-G5 and CAG-G5 electrodes. With Pt-Bi deposition, the corrosion potential dropped from −0.041 V to −0.180 V, and the corrosion current increased slightly from 1.149×10^{-5} A to 2.418×10^{-5} A, suggesting a greater tendency

toward corrosion. With the presence of Pt-Bi on the surface of the electrodes, the specific capacitance was strengthened (Fig. 1B), which accelerated the corrosion rate.

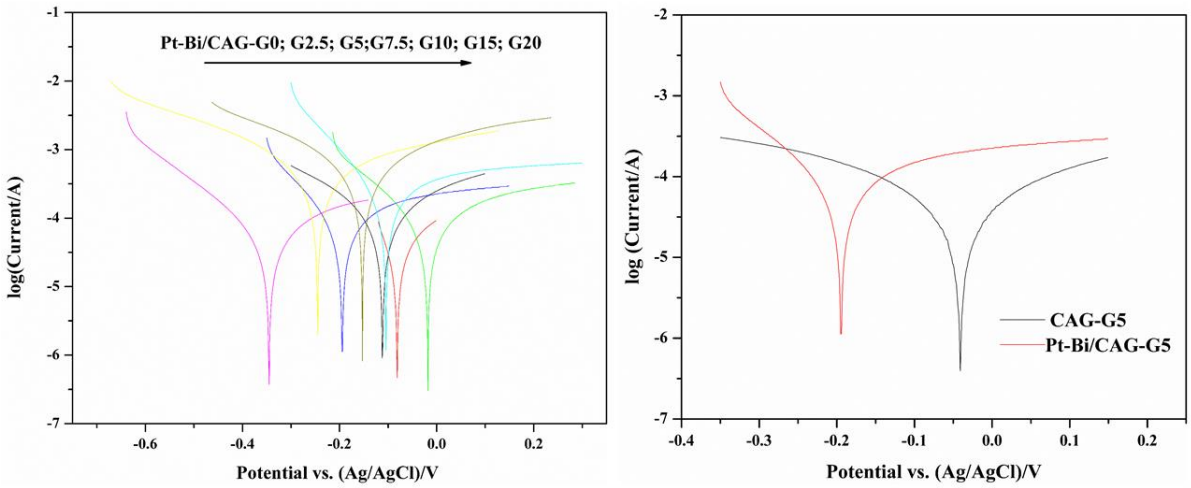

Figure 2. Polarization curves of the Pt-Bi/CAG electrodes in 0.1 M Na_2SO_4 solution. A: Pt-Bi/CAG electrodes; B: Pt-Bi/CAG-G10 and CAG-G10 electrodes (scan rate: 0.001 V s^{-1}).

The catalytic abilities of the Pt-Bi/CAG electrodes with different graphite contents and the CAG-G5 electrodes during MO degradation are shown in Fig. 3. The current densities of the Pt-Bi/CAG electrodes determined by the chronoamperometric responses under constant potentials of 1.5 V and −1.5 V were monitored for comparison. When the content of graphite powder was 5% (Pt-Bi/CAG-G5), the current density was appreciably larger than those of the other electrodes, and it was 1.5 times larger than that of Pt-Bi/CAG-G7.5. The order of the catalytic ability was extremely coincident with specific capacitance (according to Fig. 1A), indicating that catalytic ability was proportional to specific capacitance in some cases. Fig. 3B illustrates the current densities of the Pt-Bi/CAG-G5 and CAG-G5 electrodes. The Pt-Bi/CAG-G5 composite electrode showed much higher current density than CAG-G5, owing to the superior catalytic ability of Pt-Bi [25]. Compared with Li's Pt-Bi/C electrode (2.0 mA cm^{-2}) [35], the current density of the Pt-Bi/CAG-G5 electrode (1.7 mA cm^{-2}) was slightly lower in the MO solution. The CV curves of the Pt-Bi/CAG-G5 and CAG-G5 electrodes in 5 mM $[Fe(CN)_6]^{3-}/[Fe(CN)_6]^{4-}$ and 0.1 M Na_2SO_4 solutions were measured at a scan rate of 0.01V s^{-1} to examine the electrocatalytic performance of the Pt-Bi/CAG electrodes. From Fig. 3C, the inconspicuous redox peak of the CAG-G5 electrode and the significant redox peak (anodic peak at E ~ 0.39 V and cathodic peak at E ~ 0.12 V) of the Pt-Bi/CAG-G5 electrode indicated reduction/oxidation reactions in the electrolyte solution. The catalytic activity of the $Fe(CN)_6^{3-/4-}$ redox reaction was enhanced by the deposition of Pt-Bi/composite electrodes. In addition, the current density of the Pt-Bi/CAG-G5 electrode under the maximum potential (1.0 V) was higher than that of CAG-G5, further suggesting that the specific capacitance of the electrode was increased by deposition. It was found that the Pt-Bi/CAG-G5 electrode was the best one according to the electrochemical performance.

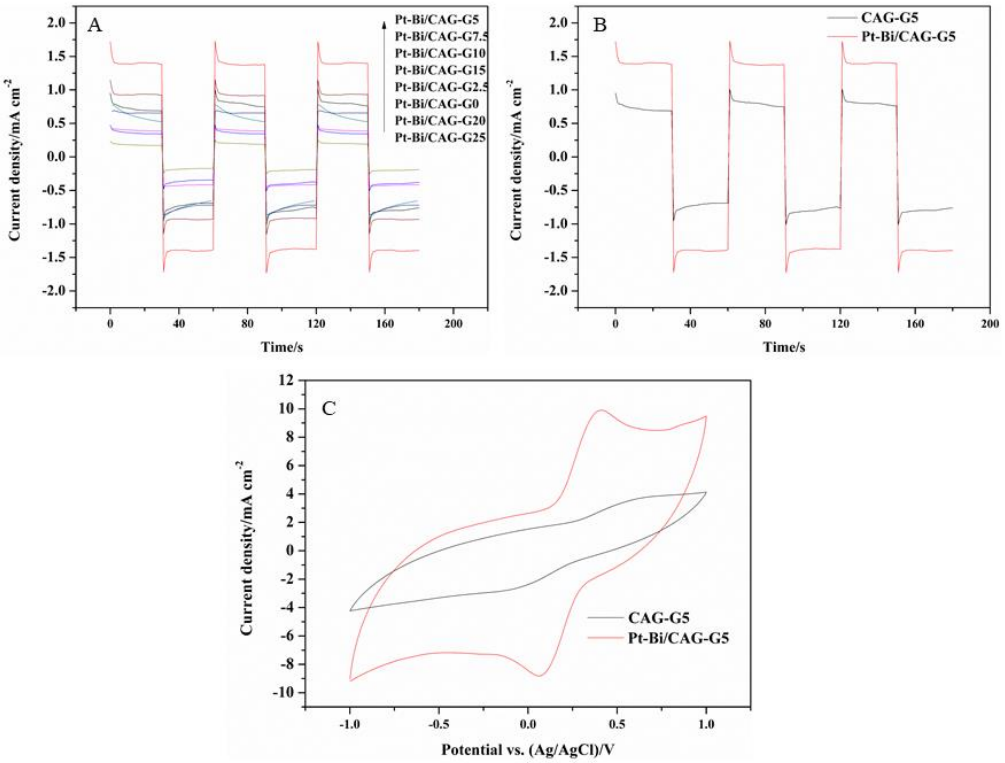

Figure 3. A: Chronoamperometric responses of the Pt-Bi/CAG electrodes in 20 mg L^{-1} MO solutions (E_U: 1.5 V; E_L: −1.5 V; duration: 1 min; E_U period/E_L period ratio: 1); B: Chronoamperometric responses of the Pt-Bi/CAG-G5 and CAG-G5 electrodes in 20 mg L^{-1} MO solutions (E_U: 1.5V; E_L: −1.5V; duration: 1 min; E_U period/E_L period ratio:1); C: CV curves of the Pt-Bi/CAG-G5 and CAG-G5 electrodes in 5 mM $[Fe(CN)_6]^{3-}$/$[Fe(CN)_6]^{4-}$ and 0.1 M Na_2SO_4 solutions at a scan rate of 0.01 V s^{-1} from -1.0 V to 1.0 V.

3.2. Characterization of the multi-layer-matrix Pt-Bi/CAG-G5 electrode

Fig. 4A shows the XRD patterns of electrodes Pt-Bi/CAG-G5 and CAG-G5. A distinct diffraction peak of graphite was observed in both the Pt-Bi/CAG-G25 and CAG-G5 patterns, indicating that graphite was not oxidized during the mixture of CAG and the deposition process. The strong diffraction peaks of calcium rosickyite (122) ($2\theta = 23.8^o$), calcium carbonate (104) ($2\theta = 29.4^o$) and calcium silicon (210) ($2\theta = 32.3^o$), as the main components of cement, were also observed in the XRD pattern of electrode CAG-G5. After electro-deposition, the diffraction peaks of Bi (012) and Pt (111) appeared at 26.9^o and 39.9^o, respectively, suggesting the successful electro-deposition of Pt and Bi particles on the CAG-G5 electrode surface. Beyond these, the diffraction peaks of calcium rosickyite (122) ($2\theta = 23.8^o$) disappeared, and the calcium carbonate peak (104) ($2\theta = 29.4^o$) was weakened after Pt-Bi was deposited. This suggests that calcium salts in the electrode can react with other substances in the electrolyte during deposition. Fig. 4B and Fig. 4C also show the existence of Pt-Bi particles that were homogeneously distributed on the multi-layer-matrix of the CAG electrode surface. The elementary composition was identified by Energy Dispersive X-ray Spectrometry (EDS), and typical Pt-Bi particles were marked with arrows.

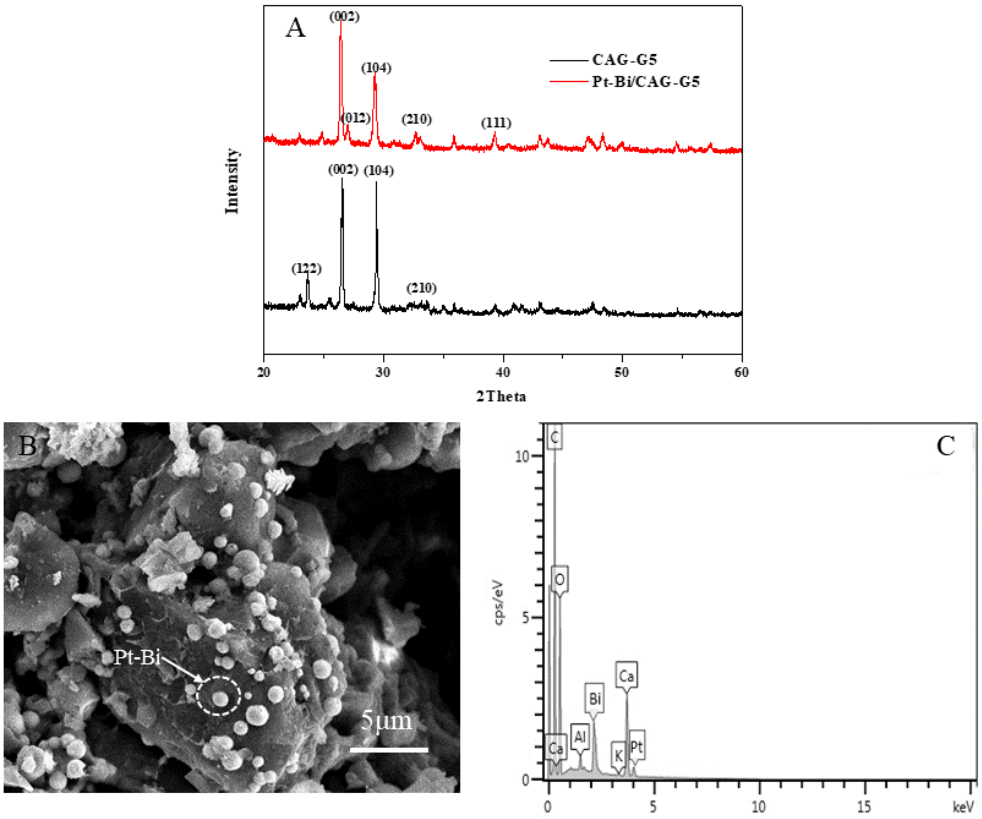

Figure 4. A: XRD patterns of Pt-Bi/CAG-G5 and CAG-G5; B: SEM image of Pt-Bi/CAG-G5; C: EDS spectrum of Pt-Bi/CAG-G5.

3.3. MO decoloration

The electrochemical catalysis performance of electrodes with different proportions was explored using the MO decoloration process. Under the pseudo-first-order kinetics condition, the kinetics equations can be fitted by the natural logarithm of the MO normalized concentration. Additionally, the correlation coefficients (r) of the fitting curves (ranging from 0.9546 to 0.9925) showed a good correlation with reaction time (Table 2), further confirming that the MO decoloration process can be described as first-order kinetics.

Experiments were conducted to investigate the influences of different electrode material ratios on MO decoloration rate. From Fig. 5A, the MO decoloration efficiencies of the Pt-Bi/CAG-C25, Pt-Bi/CAG-C30, Pt-Bi/CAG-C35, Pt-Bi/CAG-C40 and Pt-Bi/CAG-C45 electrodes were 76.62, 42.85, 22.92, 12.92 and 4.51%, respectively, after 180 min of electrolysis. The cement content had a substantial influence on the MO decoloration reaction. With increasing cement content, the content of active constituents (AC powder and graphite) decreased, which weakened the catalytic abilities of the electrodes. The water content in the electrodes may also influence the catalysis performance: approximately 76.617, 70.432, and 66.393% of the MO decoloration rate was observed with the Pt-Bi/CAG-W90, Pt-Bi/CAG-W100, and Pt-Bi/CAG-W110 electrodes, respectively (Fig. 5B). The influence of water content was small compared with that of the cement content. The change in the AC powder to graphite ratio can also affect the efficiency of MO decoloration. As seen in Fig. 5C, Pt-

Bi/CAG-G5 had the best removal rate, with a graphite rate of 5%, which accorded with the best catalytic ability of Pt-Bi/CAG-G5 electrode.

Table 2. Pseudo-first-order kinetics equations of the MO decoloration process by Pt-Bi/CAG-G electrodes in 180 min

Pt-Bi/CAG-G	kinetics equation	apparent reaction rate constant (k_{obs})	correlation coefficient (r)
G25	$\ln([MO]_0/[MO])=0.0013t+0.0427$	0.0013	0.9762
G20	$\ln([MO]_0/[MO])=0.0021t+0.0272$	0.0021	0.9925
G15	$\ln([MO]_0/[MO])=0.0052t+0.1302$	0.0052	0.9647
G10	$\ln([MO]_0/[MO])=0.0072t+0.1058$	0.0072	0.9879
G7.5	$\ln([MO]_0/[MO])=0.0074t+0.1353$	0.0074	0.9898
G5	$\ln([MO]_0/[MO])=0.0079t+0.1716$	0.0079	0.9742
G2.5	$\ln([MO]_0/[MO])=0.0038t+0.0797$	0.0038	0.9667
G0	$\ln([MO]_0/[MO])=0.0024t+0.0620$	0.0024	0.9546

The apparent reaction rate constant k_{obs} of these electrodes in the MO decoloration processes can also indicate the removal rate.

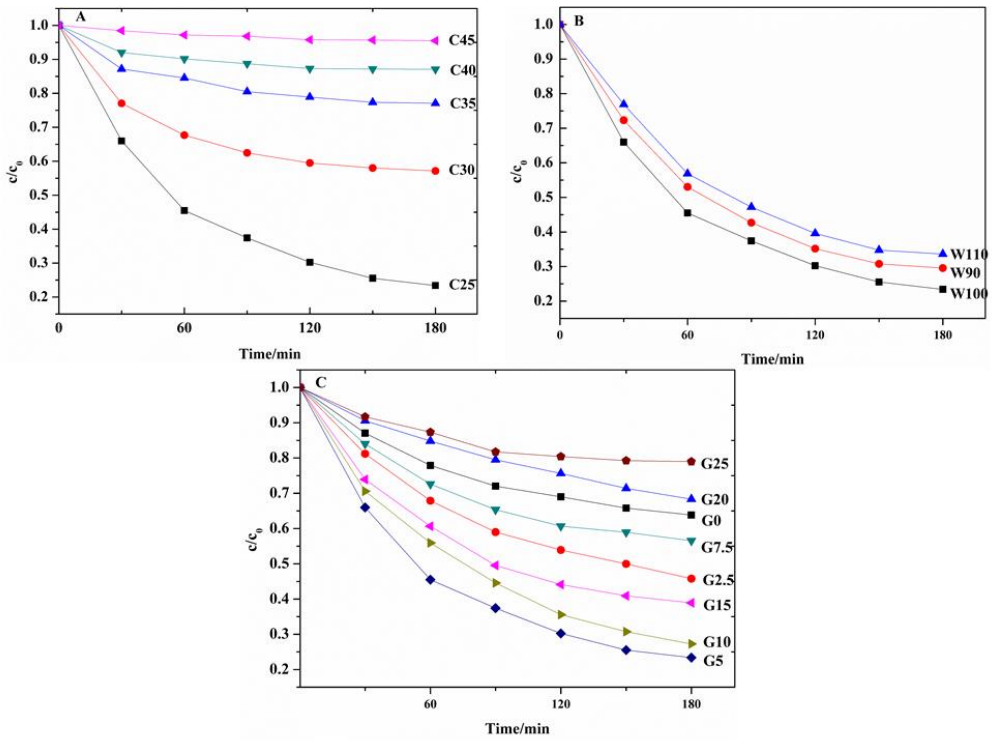

Figure 5. Decoloration efficiencies of the as-prepared samples. A: optimizing cement proportion; B: optimizing water proportion; C: optimizing graphite to AC powder proportion (initial MO concentration: 20 mg L^{-1}; E_U: 1.5V; E_L: −1.5V; period: 60 s; ratio: 1).

The apparent reaction rate constant k_{obs}, presented in Fig. 6A, increased with decreasing proportion of cement. The k_{obs} for the Pt-Bi/CAG-C25, Pt-Bi/CAG-C30, Pt-Bi/CAG-C35, Pt-Bi/CAG-

C40 and Pt-Bi/CAG-C45 samples were 0.0079, 0.0028, 0.0013, 0.0007, and 0.0003 min^{-1}, respectively, indicating that Pt-Bi/CAG-C25 was the best catalyst. In Fig. 6B, the k_{obs} for the Pt-Bi/CAG-W90, Pt-Bi/CAG-W100, and Pt-Bi/CAG-W110 electrodes were 0.0062, 0.0079, and 0.0069 min^{-1}, respectively. Fig. 6C illustrates the relationship between the apparent reaction rate constant (k_{obs}, min^{-1}) and the AC powder-to-graphite ratio. An increase in the AC powder-to-graphite ratio first led to an increase in rate and then a decrease in rate. The apparent reaction rate of Pt-Bi/CAG-G25 (k_{obs}, 0.0079 min^{-1}) was 6.077 times higher than that of Pt-Bi/CAG-G25 (k_{obs}, 0.0013 min^{-1}) and 3.292 times higher than that of Pt-Bi/CAG-G25 (k_{obs}, 0.0024 min^{-1}). Hence, considering all of the conditions, Pt-Bi/CAG-G5 (consisting of 25% cement, 5% graphite, 20% AC powder and 50% water) possessed the best MO decoloration efficiency.

To further demonstrate the effective electrocatalytic performance of the Pt-Bi/CAG-G5 composite electrode in the MO decoloration process, the TOC removal in the MO neutral solution was determined (Fig. 7A), and the MO decoloration process was monitored by UV-vis and FTIR analysis. The TOC removal rate was up to 54.80% at 180 min. Fig. 7B shows the diversification of the UV-vis spectra during the process in 180 min. The intensity of an obvious peak, which appeared at 463 nm in all spectra, declined continually, and over 76.62% of MO was decolorized within 180 min. A new peak, which appeared at 246 nm, suggested that some intermediate phase was formed, which was consistent with the FTIR spectrum (Fig. 7C). After 4 h decoloration, the intensity of the benzene ring absorption peak (1600 cm^{-1}) decreased, and the absorption peak of the N=N band (1520 cm^{-1}) disappeared; these were the characteristic bands of MO. At the same time, the spectral intensity at 3000 cm^{-1} increased significantly, and new bands appeared at 1263 cm^{-1} and 800 cm^{-1}.

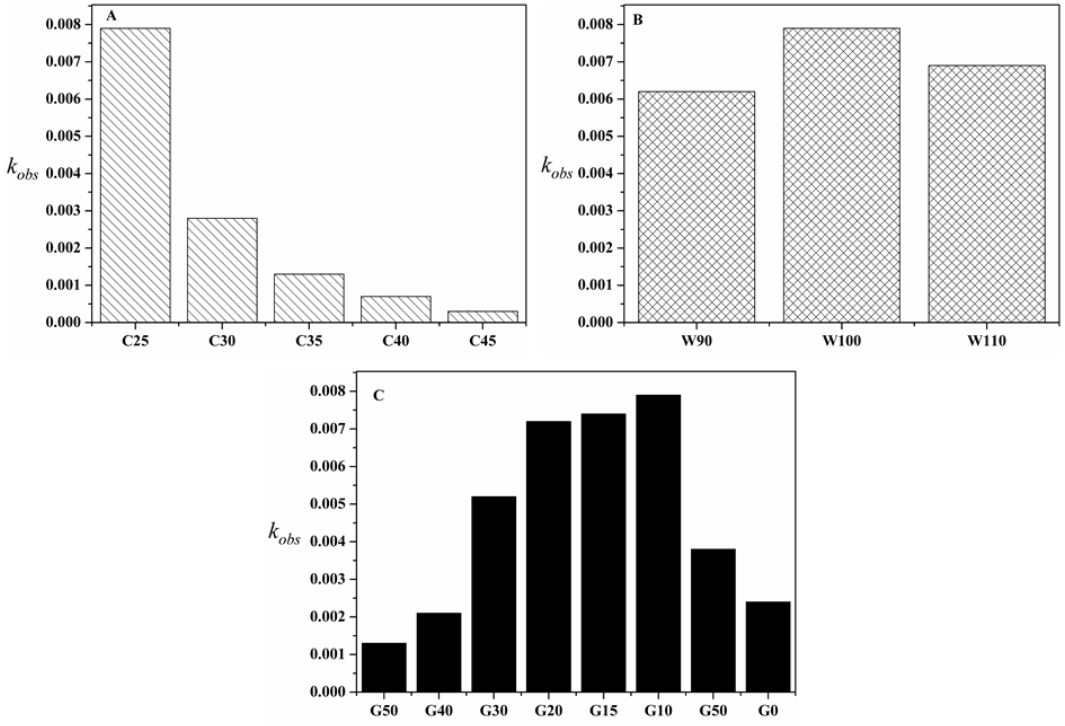

Figure 6. Evolution of the apparent reaction rate constant k_{obs}. A: as a function of cement fraction; B: as a function of water fraction; C: as a function of the graphite to AC powder fraction.

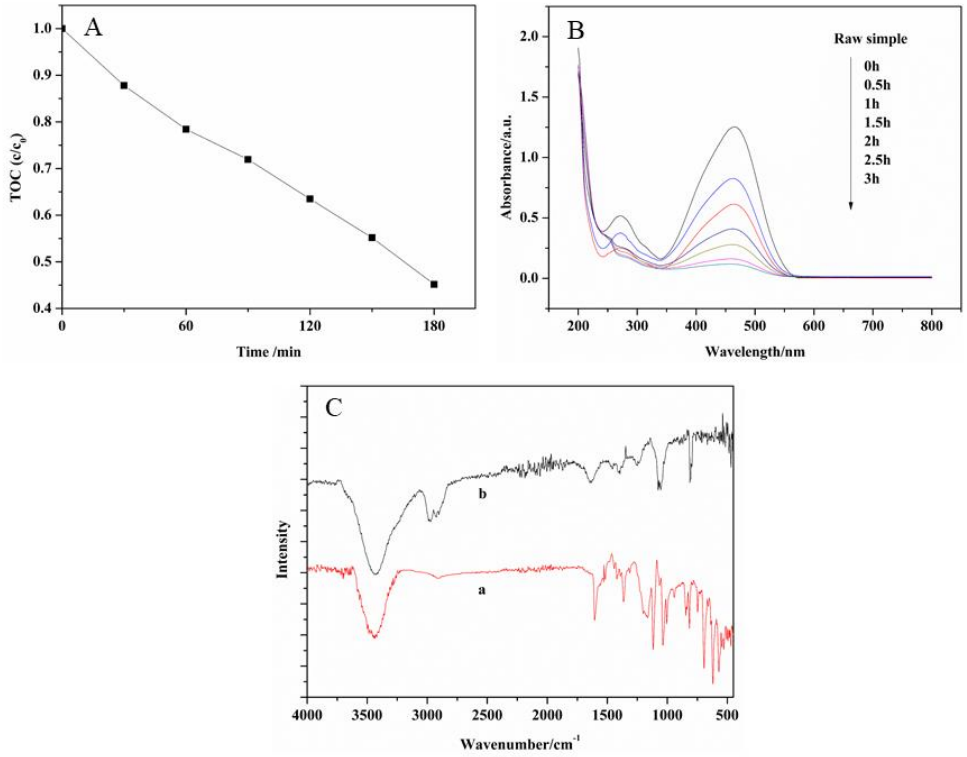

Figure 7. A: TOC removal rate by the Pt-Bi/CAG-G5 electrode; B: UV-vis spectrum evolution of the MO solution (initial MO concentration: 20 mg/L); C: FTIR spectra of the MO solution: (a) at the beginning, and (b) after 4 h of degradation (initial MO concentration: 50 mg/L; upper potential E_U: 1.5 V; lower potential E_L: −1.5 V; duration: 1 min; E_U period/E_L period ratio: 1).

3.4. Stability of Pt-Bi/CAG electrodes

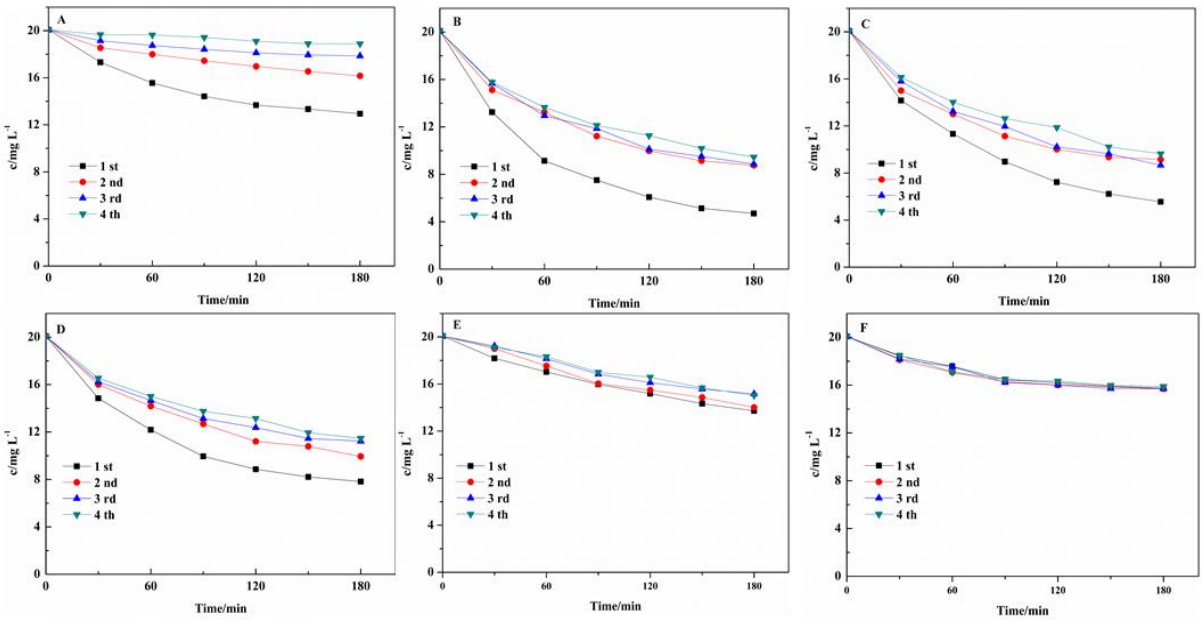

Figure 8. MO decoloration profiles with the different electrodes under a square wave potential in four consecutive electrochemical MO degradation cycles (initial MO concentration: 20 mg/L; E_U: 1.5 V; E_L: −1.5 V; period: 60 s; ratio: 1). A: Pt-Bi/CAG-G0; B: Pt-Bi/CAG-G5; C: Pt-Bi/CAG-G10; D: Pt-Bi/CAG-G15; E: Pt-Bi/CAG-G20; F: Pt-Bi/CAG-G25.

To assess the practical use of Pt-Bi/CAG electrodes, their catalytic stability was evaluated in four consecutive cycles (Fig. 8). The decoloration capacity of the graphite-free electrode decreased rapidly (Fig. 8A). For the other electrodes, the MO decoloration efficiency declined slightly in the second cycle, whereas the efficiency remained at nearly the same level in the third and fourth cycles, indicating that a good catalytic stability was observed in this system. The addition of graphite powder improved the electrochemical performance of the electrode. Based on the stable Pt-Bi/CAG-G5 electrode, the cost of the electrode synthesis was estimated and compared with other electrodes applied in MO treatment. It was found that the cost of the Pt-Bi/CAG-G5 composite electrode was the lowest, and the electro-catalytic properties were satisfied.

Table 3. Comparison of current density, MO decoloration rate, TOC removal, and cost.

	Intinal MO (mg cm^{-3})	Treated time (h)	Current density (mA cm^{-2})	MO decoloration rate (%)	TOC removal (%)	Energy cost	Cost (yuan)
Pt-Bi/CAG-G5 electrode	20	3	1.7	76.62	54.80	-	8.33
Pt-Bi/C electrode (Li et.) [35]	20	3	1.8	80	56.1	-	13.03
BDD/BDD cell [41]	100	1	500	72	-	7.66 kWh m^{-3}	~100
Nb/BDD anode [42]	100	2.3	31	96	-	7.7 kWh m^{-3}	~100
BVC/PbO_2 [44]	0.25	2	0.6	100	-	-	~200

4. CONCLUSIONS

A cost-efficient electrochemical electrode with a multi-layer matrix of cement/AC/graphite and Pt-Bi co-deposition (Pt-Bi/CAG) was synthesized. According to the SEM, EDS and XRD patterns, Pt-Bi particles were successfully deposited homogeneously on the electrode. During the comparison of electrochemical tests (including specific capacitance, corrosion resistance, catalytic performance and the MO decoloration experiment), the Pt-Bi/CAG-G5 electrode was considered to be the best one under the test conditions. This electrode was made up of 25% cement, 20% AC powder, 5% graphite and 50% water. The specific capacitance of Pt-Bi/CAG-G5 was 36.97 F cm^{-2}, which was the best value of all electrodes and was 1.103 times larger than that of the Pt-Bi/CAG-G7.5 electrode. The corresponding corrosion resistance of this electrode was one of the two best cases (Pt-Bi/CAG-G0 was the other best case), and the catalytic performance was the highest in terms of current density, which was 1.5 times larger than that of the Pt-Bi/CAG-G7.5 electrode. MO was decolored by 76.62%, and the corresponding TOC removal rate reached to 54.80% in 180 min under the square wave potential method (E_U 1.5 V, E_L −1.5 V). Also, the intensities of the UV-vis and FTIR spectra decreased during MO decoloration. Additionally, the cost of the Pt-Bi/CAG-G5 electrode was 36.05% lower compared

with the common Pt-Bi/C electrode. The Pt-Bi/CAG-G5 electrode provides an option for the dry decoloration.

ACKNOWLEDGEMENTS
This work was financially supported by the National Natural Science Foundation of China (U1662128) (No. 51678357).

References

1. M. Mirzaeian, Q. Abbas, A. Ogwu, P. Hall, M. Goldin, M. Mirzaeian and H. F. Jirandehi, *Int. J. Hydrogen Energy*, 42 (2017) 25565.
2. C.A. Martínez-Huitle, E. Brillas, *Appl. Catal*. B, 87 (2009) 105.
3. J. Sheng, C. Ma, Y. Ma, H.X. Zhang, R.R. Wang, Z.Y. Xie and J.L. Shi, *Int. J. Hydrogen Energy*, 41 (2016) 9383.
4. P.S. Fernández, A. Arenillas, E.G. Calvo, J.A. Menéndez and M.E. Martins, *Int. J. Hydrogen Energy*, 37 (2012) 10249.
5. N.P. Wickramaratne, J.T. Xu, M. Wang, L. Zhu, L.M. Dai and M. Jaroniec, *Chem. Mater*., 26 (2014) 2820.
6. K. Yuan, T. Hu, Y.Z. Xu, R. Graf, G. Brunklaus, M. Forster, Y.W. Chen and U. Scherf, *Chem. Electro. Chem.*, 3 (2016) 822.
7. Y. Zhang, G.Y. Li, Y. Lv, L.Z. Wang, A.Q. Zhang, Y.H. Song and B.L. Huang, *Int. J. Hydrogen Energy*, 36 (2011) 11760.
8. H. Chen, L. Hu, M. Chen, Y. Yan and L. Wu, *Adv. Funct. Mater*., 24 (2014) 934.
9. N. Duraisamy, A. Numan, S.O. Fatin, K. Ramesh and S. Ramesh, *J. Colloid. Interface. Sci*., 471 (2016) 136.
10. S. Shahrokhian, R. Mohammadi and E. Asadian, *Int. J. Hydrogen Energy*, 41 (2016) 17496.
11. Y.M. Chen, Z.D. Huang, H.Y. Zhang, Y.T. Chen, Z.D. Cheng, Y.B. Zhong, Y.P. Ye and X.L. Lei, *Int. J. Hydrogen Energy*, 39 (2014) 16171.
12. C. Comninellis, *Stud. Environ. Sci*., 59 (1994) 77.
13. M. A. Oturan, R. Abdelhedi, N. Oturan, M. Asma and S. Ammar, *Curr. Org. Chem*., 16 (2012) 1978.
14. C.A. Basha, R. Saravanathamizhan, V. Nandakumar, K. Chitra and W.L. Chang, *Chem. Eng. Res. Des*., 91 (2013) 552.
15. B.D. Soni, J.P. Ruparelia, *J. Environ. Res. Develop*., 8 (2013) 224.
16. M.H. Zhou, H. Särkkä and M. Sillanpää, *Sep. Purif. Technol*., 78 (2011) 290.
17. T. Panakoulias, P. Kalatzis, D. Kalderis and A. Katsaounis, *J. Appl. Electrochem*., 40 (2010) 1759.
18. M.G. Tavares, Lozele V.A. da Silva, A.M. Sales Solano, J. Tonholo, C.A. Martínez-Huitle, Carmem L.P.S. Zanta, *Chem. Eng. J.* 204-206 (2012) 141.
19. E. Pajootan, M. Arami, *Electrochim. Acta*, 112 (2013) 505.
20. H. Uehara, Y. Uemura, T. Ogawa, K. Kono, R. Ueno, Y. Niwa, H. Nitani, H. Abe, S. Takakusagi, M. Nomura, Y. Iwasawa and K. Asakura, *Phys. Chem. Chem. Phys*., 16 (2014) 13748.
21. H. Guo, H.M. Yin, X.L. Yan, S. Shi, Q.Y. Yu, Z. Cao and J. Li, *Sci. Rep*., 6 (2016) 39162.
22. B.J. Kim, K. Kwon, C.K. Rhee, J. Han and T.H. Lim, *Electrochim. Acta*, 53 (2008) 7744.
23. R. Devasenathipathy, *Int. J. Electrochem. Sci*., 11 (2016) 5441.
24. J. Sanabria-Chinchilla, H. Abe, F.J. Disalvo and H.D. Abruña, *Surf. Sci*., 602 (2008) 1830.
25. A.V. Tripkovic´, K.Dj. Popovic´, R.M. Stevanovic´, R. Socha and A. Kowal, *Electrochem. Comm*.,

8 (2006) 1492.
26. J. D. Lović, M. D. Obradović, D. V. Tripković, K. Dj. Popović, V. M. Jovanović, S. Lj. Gojković and A. V. Tripković, *Electrocatalysis*, 3 (2012) 346.
27. X.W. Yu, P.G. Pickup, *Electrochim. Acta*, 56 (2011) 4037.
28. F.A. Almarzooqi, A.A.A. Ghaferi, I. Saadat and N. Hilal, *Desalination*, 342 (2014) 3.
29. K. Yang, L. Zhu and B. Xing, *Environ. Sci. Technol*., 40 (2006) 1855.
30. J. Wang, C. Lu and J.R. Xiong, *Appl. Surf. Sci*., 298 (2014) 19.
31. P. Liu, Y.N. Gao, F.Z. Wang, W.Q. Zhang, L. Yang, J. Yang and Y.P. Liu, *Constr. Build. Mater*., 120 (2016) 42.
32. Y. Long, S. Wu, Y. Xiao, P. Cui and H. Zhou, *J. Clean Prod*., 181 (2018) 784.
33. Y. He, L. Lu, S. Jin and S. Hu, *Constr. Build. Mater*., 53 (2014) 131.
34. Y. Song, J.L. Xu and X.X. Liu, *J. Power Sources*, 249 (2014) 48.
35. S.H. Li, Y. Zhao, J. Chu, W.W. Li, H.Q. Yu and G. Liu, *Electrochim. Acta*, 92 (2013) 93.
36. L. Li, L. Zou, H. Song and G. Morris, *Carbon*, 47 (2009) 775.
37. J.C. Grunlan, W.W. Gerberich and L.F. Francis, *J. Appl. Polym. Sci.,* 80 (2001) 692.
38. H. Li, L. Pan, C.Y. Nie, Y. Liu and Z. Sun, *J. Mater. Chem.*, 22 (2012) 15556.
39. E. Herrero, A. Fernandez-Vega, J.M. Feliu, A. Aldaz, J. *Electroanal. Chem*., 350 (1993) 73.
40. J. C. Gao, S. Wu and L. Y. Qiao. *Trans. Nonferrous Met. Soc.*, 18 (2008) 588.
41. E. Isarain-Chávez, C. de la Rosa, C.A. Martínez-Huitle and J.M. Peralta-Hernández, *Int. J. Electrochem. Sci.*, 8 (2013) 3084-3094.
42. C. Ramírez, A. Saldana, B. Hernández, R. Acero, R. Guerra, S. Garcia-Segura, E. Brillas and J.M. Peralta-Hernández, *J. Ind. Eng. Chem.*, 19 (2013) 571-579.
43. Z. Liu, F. Wang, Y. Li, T. Xu and S. Zhu, *J. Environ. Sci.*, 23 (2011) S70-S73.
44. F.J. Recio, P. Herrasti, I. Sirés, A.N. Kulak, D.V. Bavykin, C. Ponce-de-León and F.C. Walsh, *Electrochim. Acta*, 56 (2011) 5158-5165.